Molecular Therapy
Nucleic Acids
Original Article

Cathepsin B-activatable cyclic antisense oligonucleotides for cell-specific target gene knockdown *in vitro* and *in vivo*

Zhongyu Wang,[1,3] Xinli Fan,[1,3] Guanqun Mu,[1] Xiaoran Zhao,[1] Qian Wang,[1] Jing Wang,[1] and Xinjing Tang[1,2]

[1]State Key Laboratory of Natural and Biomimetic Drugs, School of Pharmaceutical Sciences and Chemical Biology Center, Peking University, No. 38, Xueyuan Road, Beijing 100191, People's Republic of China; [2]State Key Laboratory of Pharmaceutical Biotechnology, Nanjing University, Nanjing, Jiangsu 210023, People's Republic of China

Trigger-activatable antisense oligonucleotides have been widely applied to regulate gene function. Among them, caged cyclic antisense oligonucleotides (cASOs) maintain a specific topology that temporarily inhibits their interaction with target genes. By inserting linkers that respond to cell-specific endogenous stimuli, they can be powerful tools and potential therapeutic agents for specific types of cancer cells with low off-target effects on normal cells. Here, we developed enzyme-activatable cASOs by tethering two terminals of linear antisense oligonucleotides through a cathepsin B (CB) substrate peptide (Gly-Phe-Leu-Gly [GFLG]), which could be efficiently uncaged by CB. CB-activatable cASOs were used to successfully knock down two disease-related endogenous genes in CB-abundant PC-3 tumor cells at the mRNA and protein levels but had much less effect on gene knockdown in CB-deficient human umbilical vein endothelial cell (HUVECs). In addition, reduced nonspecific immunostimulation was found using cASOs compared with their linear counterparts. Further *in vivo* studies indicated that CB-activatable cASOs showed effective tumor inhibition in PC-3 tumor model mice through downregulation of translationally controlled tumor protein (TCTP) protein in tumors. This study applies endogenous enzyme-activatable cASOs for antitumor therapy in tumor model mice, which demonstrates a promising stimulus-responsive cASO strategy for cell-specific gene knockdown upon endogenous activation and ASO prodrug development.

INTRODUCTION

Cyclic oligonucleotides are important in regulating biological processes and are used as potential biomarkers in disease diagnosis.[1–3] They have also been developed as powerful tools in regulating gene expression.[4–9] Over the past few decades, photolabile cyclic oligonucleotides have been developed as excellent scientific tools to investigate and evaluate gene function with high spatiotemporal resolution at the cellular and animal levels using light as an external trigger.[10–16] However, light-triggered activation of photolabile oligonucleotide tools in complex three-dimensional morphology remains challenging. Fortunately, endogenous stimuli[17] can also be utilized to trigger caged cyclic oligonucleotides. Yamazoe et al.[18] explored nitroreductase-activated cyclic morpholino oligonucleotide probes to study gene function regulation during embryonic development in zebrafish, and Yang et al.[19,20] described a caspase-3-activated cyclic hairpin oligonucleotide probe for detection of caspase-3 activity during apoptosis. Currently there is no study to knockdown the disease-related target genes using enzyme-activatable circular antisense oligonucleotides in cancer therapy. Among many endogenous stimuli, cancer-related proteases have been widely used as enzyme-sensitive sensors and prodrugs for disease diagnosis[21] and tumor therapy,[22] including controllable release of drugs[23–25] and selective delivery of biomacromolecules.[26,27] Cathepsin B (CB), a lysosomal cysteine protease, is highly expressed in many cancer cells (such as prostate cancer [PC-3] cells).[28] Accordingly, CB is recognized as an important biomarkers for the occurrence and progression of many cancers[29] and a suitable endogenous stimulus for activating prodrugs in cancer therapy. A tetrapeptide (Gly-Phe-Leu-Gly [GFLG]) has been identified as a specific substrate for CB and has been widely applied as a CB-cleavable moiety in sensors and prodrugs.[30]

Here, we designed and synthesized CB-activatable cyclic antisense oligonucleotides (cASO-CBs) by tethering the 3′ and 5′ terminals of ASOs with CB-cleavable GFLG tetrapeptide linkers (Figure 1). These cASO-CBs were inert to bind target mRNAs until the tetrapeptide linker was cleaved by CB to recover the corresponding linear ASOs. A large difference in cASO-induced cell-specific target gene knockdown was successfully achieved between CB-rich PC-3 cancer cells and CB-deficient normal human umbilical vein endothelial cells (HUVECs) or small interfering RNA $(siRNA)_{CB}$-silenced PC-3 cells. Endogenous stimulus-sensitive cASOs also showed promise for specific activation of cASO prodrugs in specific cancer cells and tumors *in vivo*, with few off-target effects and nonspecific immunostimulation.

Received 19 October 2022; accepted 20 July 2023;
https://doi.org/10.1016/j.omtn.2023.07.022.

[3]These authors contributed equally

Correspondence: Xinjing Tang, State Key Laboratory of Natural and Biomimetic Drugs, School of Pharmaceutical Sciences and Chemical Biology Center, Peking University, No. 38, Xueyuan Road, Beijing 100191, People's Republic of China.
E-mail: xinjingt@bjmu.edu.cn

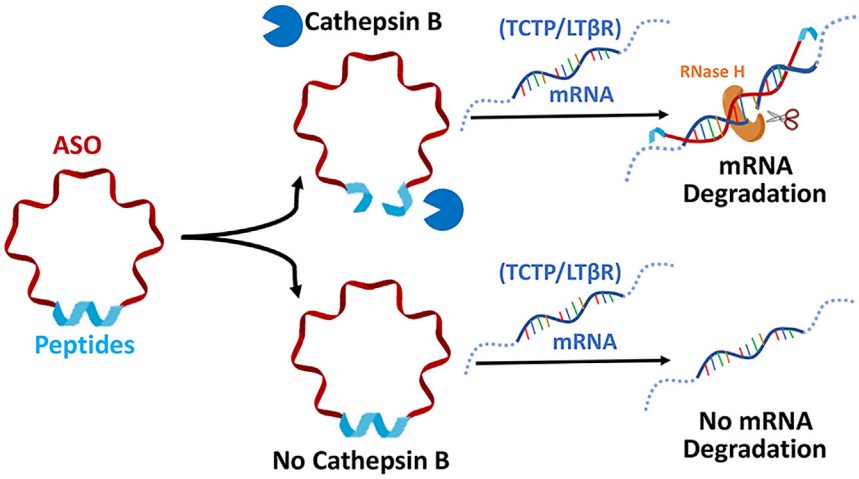

Figure 1. Gene knockdown of cASO-CBs

RESULTS

Rational design and synthesis of cASO-CBs

To construct caged cASO-CBs, the 3′ and 5′ terminals of ASOs were tethered with a CB-cleavable peptide (GFLG) through click chemistry (Figure 2). The antisense phosphorothioated oligonucleotides were synthesized with 3′-amino-modified C7 controlled pore glass (CPG), followed by coupling of the C6-NHS phosphoramidite linker (linker 1, as shown in Figure S1) at their 5′ terminals to afford **1**. The CB-cleavable linker (heptynyl-GFLGK-NH_2, **2a**) containing a heptynyl moiety was conjugated to the 5′ terminal of the oligonucleotides through amide formation between an amino group of the peptide and a carboxylic N-hydroxysuccinimide (NHS) ester of the oligonucleotide on solid-phase resin. After deprotection and purification, the obtained oligonucleotide-peptide conjugates (**3a**) with a 3′ amino moiety were coupled with 3-azidopropanoic acid NHS ester (linker 2, as shown in Figure S1) to obtain linear ASO (lASO)-CB (**4a**) with alkyne and azide moieties at the 5′ and 3′ terminals, respectively.

The final cASO-CBs (targeting translationally controlled tumor protein [TCTP] or lymphotoxin-β receptor [LTBR]) were obtained through click cyclization between the azido and alkynyl moieties of two terminals of ASOs. Relatively high cyclization yields (~65%) were achieved, probably because of the relatively low oligonucleotide concentration and 6-bp stem of ASOs. After further high performance liquid chromatography (HPLC) purification (Figures S2B and S2C), $cASO_{TCTP}$-CB and $cASO_{LTBR}$-CB were confirmed by 20% native PAGE gel analysis and mass spectrometry (MS) characterization (Table S1). In addition, a non-CB-sensitive $cASO_{TCTP}$-GGGG was also synthesized as a negative control by replacing the CB-sensitive GFLG peptide substrate with a CB -insensitive GGGG tetrapeptide.[31,32] $cASO_{TCTP}$-GGGG was synthesized, purified, and characterized using the same procedure as for $cASO_{TCTP}$-CB (Figure S2D).

Enzymatic uncaging of $cASO_{TCTP}$-CB with CB in solution

Enzymatic uncaging of cyclic $cASO_{TCTP}$-CB was investigated with DTT-preactivated CB (1 μg/mL) in 4-morpholineethanesulfonic acid (MES) buffer (pH 5) at 37°C for 1 h. Successful cleavage of the CB-sensitive peptide substrate was observed with the appearance of a slower-moving band than that of the cASO (Figure 3A). Grayscale quantitative analysis indicated that more than 90% of the lASO was recovered within 1 h of incubation. In addition, CB enzymatic activity for $lASO_{TCTP}$-CB or $cASO_{TCTP}$-CB was measured at concentrations of 0.5, 1, 2, and 4 μM under preactivated CB (1 μg/mL) in MES buffer (pH 5) at 37°C for 1 h. Then, the Km values were calculated according to the grayscale quantitative analysis of cleaved bands on the PAGE gels by the Lineweaver-Burk plot (Figure S3). The Km value of CB for $cASO_{TCTP}$-CB (~0.51 μM) did not appear to be significantly different from that of $lASO_{TCTP}$-CB (~0.46 μM), indicating that the peptide linker in cASO could be cleaved by CB as effectively as that in lASO and that the cyclic loop of $cASO_{TCTP}$-CB has little effect on CB peptide cleavage activity. To confirm the specificity of CB-induced uncaging of cyclic oligonucleotide, leupeptin, an inhibitor of CB,[33] was pre-added to the reaction mixture at leupeptin concentrations of 0.25, 2, 4, and 10 μM (Figure 3B). The presence of only 0.25 μM leupeptin resulted in efficient inhibition of CB cleavage activity. In addition, for nonspecific enzymes such as caspase-3 and peptidase, obvious cleavage of the peptide linker (GFLG) of $cASO_{TCTP}$-CB was not observed (Figure S4). For the non-CB-sensitive $cASO_{TCTP}$-GGGG, CB did not obviously induce its cleavage, while $cASO_{TCTP}$-CB was effectively uncaged by CB under the same conditions (Figure S5). These results indicated the specific uncaging ability of CB.

The binding affinity of ASO_{TCTP} or $cASO_{TCTP}$-CB to target RNA

A 46-mer Cy5-labeled RNA oligonucleotide (Cy5-RNA) truncated from the TCTP mRNA sequence was synthesized for the affinity assay. Microscale thermophoresis (MST) was applied to examine the affinity of ASO_{TCTP} and $cASO_{TCTP}$-CB for the target Cy5-RNA. As shown in Figure S6, the MST results indicated that the K_D value of $lASO_{TCTP}$/Cy5-RNA (0.024 ± 0.004 μM) was much lower than that of the cyclic $cASO_{TCTP}$-CB/Cy5-RNA (5.194 ± 0.272 μM), indicating that the cyclic structure of $cASO_{TCTP}$-CB greatly inhibited its binding to the target Cy5-RNA compared with $lASO_{TCTP}$. The affinity of lASO-CB for Cy5-RNA (Figure S6) was also tested, and the K_D value of lASO-CB/Cy5-RNA (0.027 ± 0.001 μM) was close to that of lASO/Cy5-RNA (0.068 ± 0.001 μM). These results indicated that the peptide part of lASO-CB barely affected the binding between lASO-CB and target Cy5-RNA. These results indicated that these cyclic oligonucleotides would be expected to reduce binding to off-target transcripts, which could reduce the off-target effect of antisense therapy.

RNase H1-induced target RNA digestion using ASO_{TCTP} and $cASO_{TCTP}$-CB

RNase H1-mediated cleavage of target RNA with $cASO_{TCTP}$-CB was examined before and after CB activation. A 46-mer Cy3-labeled RNA

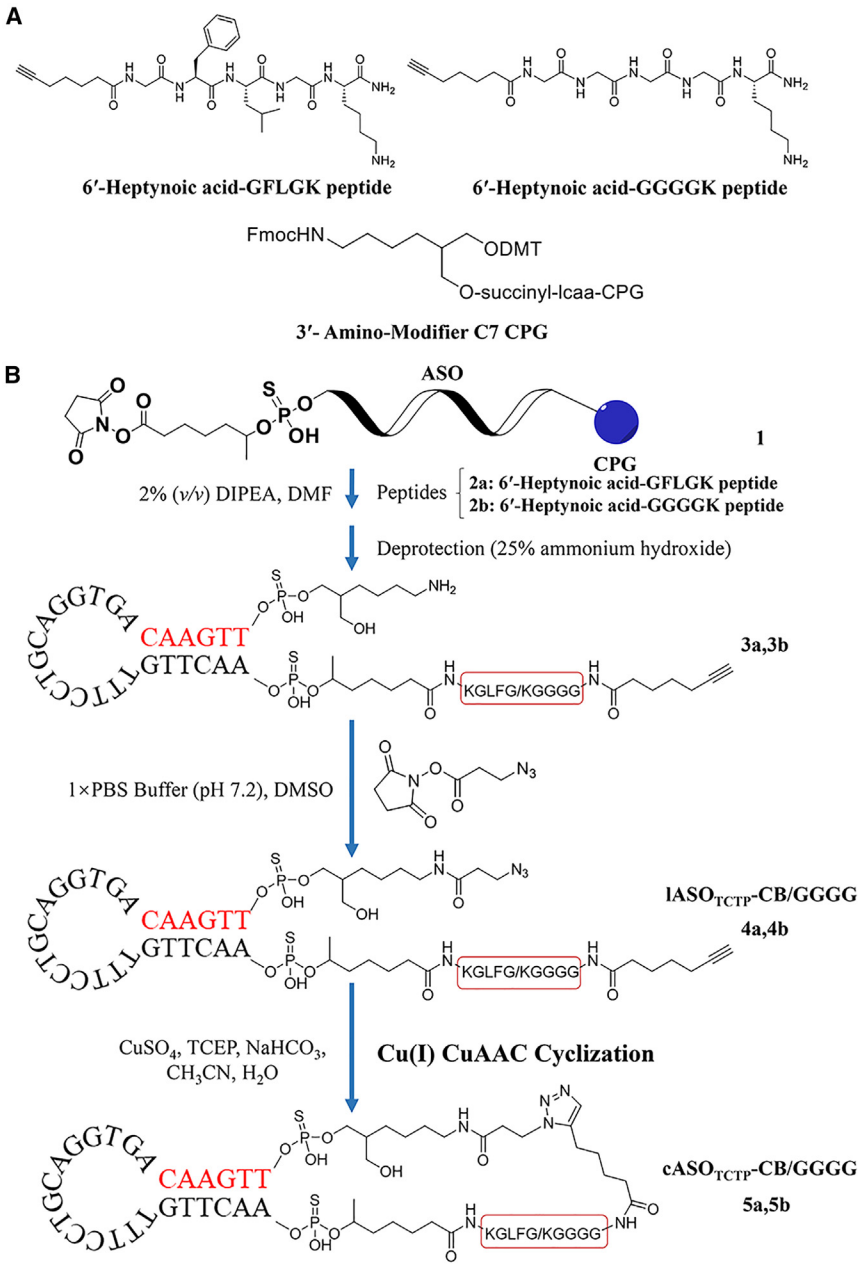

Figure 2. Schematic illustration of synthetic cyclic ASO modified with peptides

(A) The structural formula of two peptide linkers and the 3′-amino-modifier C7 CPG used in cyclization. (B) The cyclization process of cyclic cASO-CB/cASO-GGGG.

oligonucleotide (Cy3-RNA) truncated from the TCTP mRNA sequence was synthesized as the target RNA oligonucleotide for the RNase H1 assay. At a ratio of Cy3-RNA to ASO of 40:1 (4 μM Cy3-RNA and 0.1 μM template ASO), up to 22.5-fold enhancement of target RNA cleavage with CB-pretreated $cASO_{TCTP}$-CB was successfully achieved in comparison with the caged $cASO_{TCTP}$-CB. Compared with $lASO_{TCTP}$, the recovery rate of RNA cleavage after CB activation of $cASO_{TCTP}$-CB was approximately 70% (Figures 3C, 3D, and S7). The incomplete recovery of RNA cleavage by $cASO_{TCTP}$-CB compared with $lASO_{TCTP}$ was probably caused by interference from the previous CB cleavage system. The low leaky RNA cleavage (less than 2%) in lane 3 indicated that the CB-sensitive $cASO_{TCTP}$-CB had a good caging effect on RNase H1-mediated cleavage of target RNA, similar to the previous photolabile cyclic ASOs.[34] These results indicated that CB induced enzymatic uncaging of $cASO_{TCTP}$-CB and restored the corresponding lASO, which apparently recovered RNA/ASO duplex formation, and the following RNase H1-induced cleavage of target RNA.

TCTP gene knockdown with CB-activatable $cASO_{TCTP}$-CB in cells

The TCTP gene is extensively expressed in many cancers, including prostate cancer.[35] Reduction of TCTP in PC-3 cells could induce inhibition of PC-3 cell growth.[35] The dose-dependent effect of $cASO_{TCTP}$-CB on TCTP knockdown was first examined at 48 h at concentrations of 30, 60 and 100 nM (Figure 4A). $lASO_{TCTP}$ and $cASO_{TCTP}$-CB induced effective TCTP knockdown (71% and 57%, respectively) at 30 nM. At higher concentrations of ASOs (100 nM), there was no significant difference in downregulation of TCTP mRNA levels between $lASO_{TCTP}$ (82%) and $cASO_{TCTP}$-CB (75%). Time-dependent knockdown of TCTP mRNA levels was investigated from 24–60 h with 100 nM $lASO_{TCTP}$ and $cASO_{TCTP}$-CB in PC-3 cells (Figure 4B). $lASO_{TCTP}$ induced a quick reduction in TCTP mRNA levels compared with $cASO_{TCTP}$-CB at 24 h, as expected. Thereafter, the TCTP mRNA level in PC-3 cells gradually increased with a longer incubation time using $lASO_{TCTP}$. However, for $cASO_{TCTP}$-CB, a gradual reduction of TCTP mRNA level was observed from 30% at 24 h to 25% at 60 h. Based on these results, $cASO_{TCTP}$-CB could be gradually uncaged by cellular CB, which induced slightly slower downregulation of the target TCTP gene than $lASO_{TCTP}$, as expected. In comparison with lASOs, long-term gene knockdown was observed for cASO, probably because of the higher stability and gradual enzymatic uncaging of cASOs. In addition, PC-3 cells were treated using 100 nM $lASO_{Nonsense}$ and $cASO_{Nonsense}$-CB with or without Lipofectamine 2000 transfection reagent. Neither of the control nonsense ASOs caused TCTP mRNA downregulation with the aid of transfection reagent at 48 h (Figure S8).

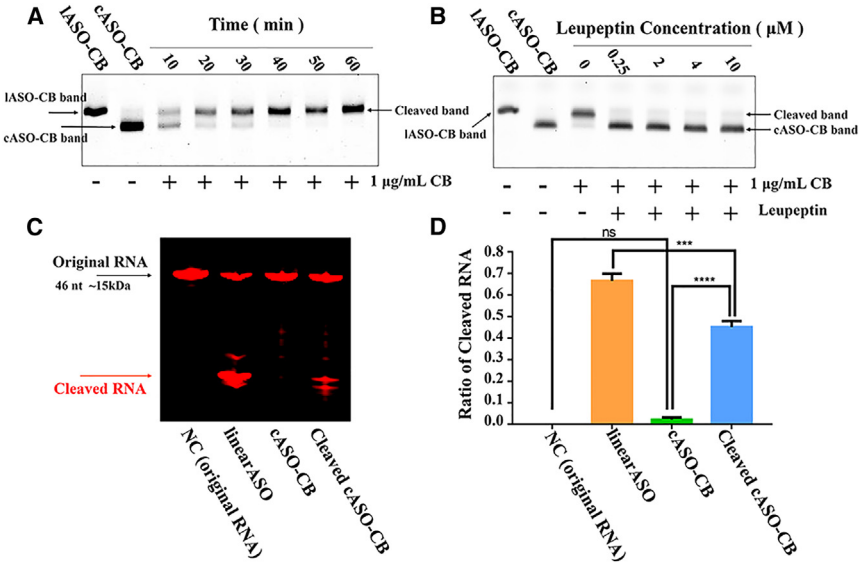

Figure 3. CB triggered cleavage of cASO-CB and the following degradation of complementary RNA oligonucleotides by RNase H1

(A) Time dependence of cASO-CB uncaging with incubation of CB (1 μg/mL) at 37°C. (B) Concentration dependence of leupeptin on CB activity for cASO-CB uncaging. (C) RNase H1 induced cleavage of the Cy3-labeled 46-mer RNA oligonucleotide using cASO-CB and RNase H1 at 37°C. (D) Quantitative analysis of RNA cleavage from (C). All quantitative data are presented as mean ± SEM ($n \geq 3$), ***$p < 0.001$, ****$p < 0.0001$.

To investigate the cell-specific effect of $cASO_{TCTP}$-CB on TCTP gene knockdown, CB-abundant PC-3 cancer cells and CB-deficient HUVECs were used (Figures S9 and S10). No significant difference in TCTP mRNA levels was found in PC-3 cells using $lASO_{TCTP}$ (18%) and $cASO_{TCTP}$-CB (25%) at 100 nM concentration in 48 h (Figure 4C). Similar protein levels of TCTP were also achieved at 48 h between $lASO_{TCTP}$ treatment (40%) and $cASO_{TCTP}$-CB treatment (47%) (Figures 4D and 4E). In HUVECs, a clear difference in TCTP mRNA expression was observed between $lASO_{TCTP}$ (43%) and $cASO_{TCTP}$-CB (63%) at 100 nM (Figure 4C). More significant differences in TCTP protein levels were found in CB-deficient HUVECs. As seen in Figures 4D and 4E, $cASO_{TCTP}$-CB only induced less than 1/3 of TCTP protein knockdown (~20% vs. 65%) in comparison with $lASO_{TCTP}$ in HUVECs, which indicated that $cASO_{TCTP}$-CB was not efficiently uncaged in CB-deficient HUVECs.

To confirm CB-specific activation of $cASO_{TCTP}$-CB in PC-3 cells, expression of CB in PC-3 cells was also suppressed through pretreatment with 100 nM $siRNA_{CB}$ as well as a scramble siRNA as a control (Figures S10 and S11). After 36 h of pre-transfection of CB siRNA into PC-3 cells, $cASO_{TCTP}$-CB or ASO_{TCTP} was transfected. Unsurprisingly, qRT-PCR results of TCTP mRNA indicated that TCTP knockdown using 100 nM $cASO_{TCTP}$-CB was clearly inhibited in CB-suppressed PC-3 cells (~18% reduction) in comparison with that of the control group with scramble siRNA-treated PC-3 cells (~43% reduction). There was no obvious difference in TCTP gene knockdown with treatment of $lASO_{TCTP}$ between the CB-suppressed PC-3 cells (~45% reduction) and normal control PC-3 cells (~47% reduction) (Figure S12). For further comparison and identification, gene knockdown of TCTP was also evaluated in PC-3 cells with a non-CB-sensitive control ASO, $cASO_{TCTP}$-GGGG (Figure S13). With increased concentration of $cASO_{TCTP}$-GGGG in PC3 cells, there was a certain leakage knockdown of TCTP mRNA expression, which may be caused by nonspecific degradation of the GGGG linker with intracellular hydrolase. However, under the same working concentration of 100 nM, the expression of TCTP mRNA in $cASO_{TCTP}$-CB was 2.5-fold lower than in $cASO_{TCTP}$-GGGG, further confirming that CB-specific GFLG linkage is the key point for efficiency of ASO activation and subsequent effective gene silencing in PC-3 cells. These data strongly indicated that $cASO_{TCTP}$-CB was truly cleaved by the high level of CB in PC-3 cells and that the released linear counterpart then induced effective target gene silencing.

LTBR gene knockdown with $cASO_{LBR}$-CB

To demonstrate the generalizability of the enzyme-activatable cASO strategy, another disease-related endogenous LTBR gene associated with inflammation-induced carcinogenesis was chosen.[36] Knockdown of LTBR has already been utilized in several anti-inflammatory and anticancer studies.[37,38] As shown in Figure 5A, $cASO_{LTBR}$-CB and $lASO_{LTBR}$ induced effective knockdown of target LTBR mRNA in a dose-dependent manner. About 61% reduction in LTBR mRNA was observed with 30 nM $cASO_{LTBR}$-CB during 48 h incubation, which was close to that of $lASO_{LTBR}$ (65%). Increasing the ASO concentration to 100 nM resulted in more effective mRNA knockdown with $cASO_{LTBR}$-CB (72%) and ASO_{LTBR} (78%) treatment. The time-dependent effect of LTBR mRNA levels was also evaluated with ASO_{LTBR} and $cASO_{LTBR}$-CB at 30 nM in PC-3 cells. As shown in Figure 5B, $lASO_{LTBR}$ and $cASO_{LTBR}$-CB showed gradually enhanced gene silencing effects from 12–48 h, with only a slight increase in mRNA levels at 60 h post transfection. This observation indicated that $cASO_{LTBR}$-CB could also be successfully uncaged from the cyclic structure under activation of CB in PC-3 cells and further downregulated the target LTBR gene. In addition to LTBR mRNA levels, LTBR protein levels were also efficiently downregulated with 100 nM $cASO_{LTBR}$-CB treatment (30%) in 48 h, which was more efficient than $lASO_{LTBR}$ treatment (40%) (Figures 5C and 5D). Thus, $cASO_{LTBR}$-CB maintained similar or even better knockdown of the target LTBR gene at the mRNA and protein levels in CB-rich PC-3 cells, which further confirmed that the enzyme-activatable cASO strategy had generality for knockdown of different target genes upon endogenous enzymatic activation.

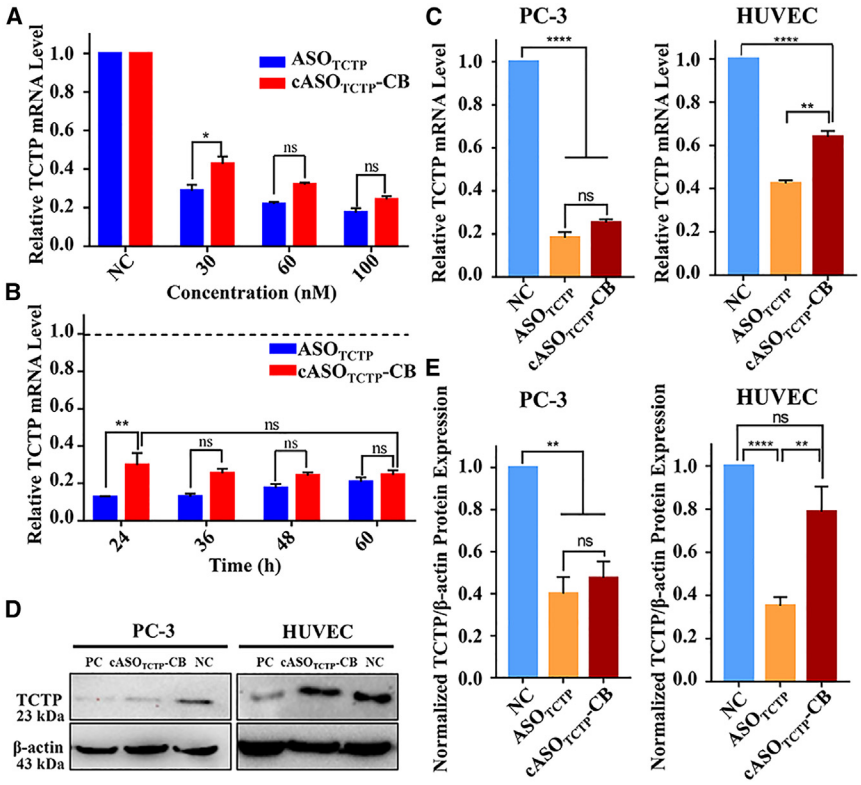

Figure 4. Knockdown of TCTP gene expression with cASO$_{TCTP}$-CB in PC-3 cells and HUVECs

(A) Concentration dependence of TCTP mRNA knockdown with ASO$_{TCTP}$ and cASO$_{TCTP}$-CB in PC-3 cells at 48 h. (B) Time dependence of TCTP mRNA knockdown with 100 nM ASO$_{TCTP}$ and cASO$_{TCTP}$-CB, respectively, in PC-3 cells. (C) Relative quantification of TCTP mRNA levels transfected in CB-abundant PC-3 cells and CB-deficient HUVECs with cASO$_{TCTP}$-CB and ASO$_{TCTP}$ (100 nM) at 48 h normalized to β-actin. (D) Western blotting analysis of TCTP expression in PC-3 cells and HUVECs treated with 100 nM cASO$_{TCTP}$-CB and ASO$_{TCTP}$. (E) Relative quantification of TCTP protein levels normalized to β-actin protein using ImageJ software. The ASOs used in cellular experiments were transfected by Lipofectamine 2000. "NC" refers to the group treated with Lipofectamine 2000 only. All data are presented as mean ± SEM (n ≥ 3). *p < 0.05, **p < 0.01, ****p < 0.0001.

Nonspecific immune response of cASO-CBs in PC-3 cells

Nonspecific immunity is one of the key side effects of ASO therapy because of activation of Toll-like reporters.[39–43] Thus, nonspecific immunostimulation of cASO-CB was also investigated compared with its corresponding lASO in PC-3 cells. 100 nM cASO$_{TCTP}$-CB and lASO$_{TCTP}$ were transfected into PC-3 cells, and four typical immune indicators, interleukin-6 (IL-6), interferon-β (IFN-β), Toll-like receptor 9 (TLR9), and IFN regulatory factor 7 (IRF7), were evaluated. As shown in Figure 6A, lASO$_{TCTP}$ induced an approximately 3.5-fold increase in IL-6 mRNA levels compared with the negative control (NC) group, whereas cASO$_{TCTP}$-CB resulted in only 1.7-fold enhancement. In comparison with the NC group, a nearly 8-fold enhancement of IFN-β mRNA (Figure 6B) in lASO-treated cells was observed, while a much more modest increase in IFN-β mRNA (∼2-fold) was observed with cASO$_{TCTP}$-CB transfection, an approximately 4-fold decrease in immunostimulation. A similar phenomenon was also observed for detection of TLR9 and IRF7 mRNA levels. cASO$_{TCTP}$-CB also induced lower RNA level increases than lASO$_{TCTP}$ (Figures 6C and 6D). These results indicated that the nonspecific immunogenicity of cASO$_{TCTP}$-CBs was significantly lower than that of lASO$_{TCTP}$, and it had obvious advantages in reducing the inherent off-target effects caused by the immunogenicity of ASOs.

In vivo TCTP gene silencing and antitumor effect with cASO$_{TCTP}$-CBs in a xenograft tumor model

Based on the cellular results, the gene knockdown and antitumor effects of cASO$_{TCTP}$-CBs were evaluated in nude mice bearing PC-3 cells. Throughout the experiment, no obvious difference was observed in the body weight of mice in all experimental groups (Figure S14). As expected, lASO$_{TCTP}$ obviously inhibited tumor growth in comparison with the NC (Figure 7A). Fortunately, cASO$_{TCTP}$-CB treatment also induced tumor growth inhibition that was similar to lASO$_{TCTP}$ treatment, indicating that cASOs were successfully uncaged to degrade mRNA in CB-rich PC-3 tumors. However, the tumor volumes of mice in the cASO$_{TCTP}$-GGGG-treated group still increased gradually and were similar to those of the NC group because of the non-CB-sensitive GGGG linkage. In addition, weight analysis of harvested tumors also revealed that cASO$_{TCTP}$-CB treatment apparently decreased the tumor weight a little bit more than lASO$_{TCTP}$ treatment, while a small decrease in tumor weight with NC and CB-insensitive cASO$_{TCTP}$-GGGG treatment could be observed (Figures 7B and S15). All of these data indicated that cASO$_{TCTP}$-CB was cell-specifically activated in CB-rich PC-3 tumors and displayed the same potent inhibition of tumor growth as lASO$_{TCTP}$.

To identify the molecular level of target gene downregulation by cASO$_{TCTP}$-CBs in tumors, TCTP protein levels were also evaluated in the corresponding tumor tissues. Western blot analysis of TCTP protein in tumors confirmed that ASO$_{TCTP}$ (57%) and cASO$_{TCTP}$-CB (71%) induced downregulation of TCTP protein in PC-3 tumors compared with the NC group, whereas the non-CB-sensitive cASO$_{TCTP}$-GGGG roughly maintained a similar level of TCTP protein as the NC (Figures 7C and 7D). The tumor slices were then subjected to H&E staining and TCTP immunohistochemistry (IHC) staining. As shown in Figure 7E, compared with to the NC groups, tumor slides from ASO$_{TCTP}$ and cASO$_{TCTP}$-CB-treated mice had large areas of aggregation and degradation of dead cells. IHC staining of TCTP protein also indicated that ASO$_{TCTP}$ and cASO$_{TCTP}$-CB treatment exhibited

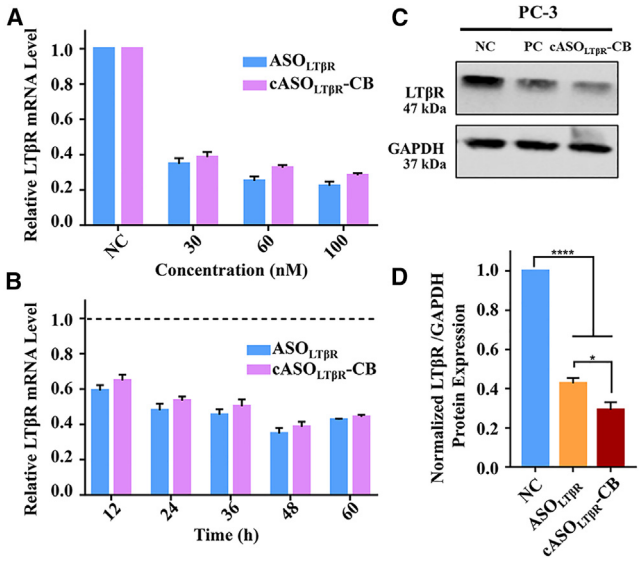

Figure 5. Knockdown of LTBR gene expression with cASO$_{LTBR}$-CB in PC-3 cells

(A) Concentration dependence of LTBR mRNA knockdown with ASO$_{LTBR}$ and cASO$_{LTBR}$-CB in 48 h. (B) Time dependence of LTBR mRNA knockdown with 30 nM ASO$_{LTBR}$ and cASO$_{LTBR}$-CB. (C) Western blotting analysis of LTBR protein level treated with 100 nM ASO$_{LTBR}$ and cASO$_{LTBR}$-CB for 48 h. (D) Relative quantified analysis of LTBR protein levels normalized to GAPDH protein using ImageJ. The ASOs were transfected by Lipofectamine 2000. All data are presented as mean ± SEM ($n \geq 3$). *$p < 0.05$, ****$p < 0.0001$.

efficient knockdown of TCTP protein in tumor tissues compared with the NC group, confirming that TCTP gene knockdown could achieve selective and effective cancer cell death when cASO$_{TCTP}$-CB was triggered by a high level of endogenous CB in PC-3 tumors.

DISCUSSION

In summary, we rationally developed cASO-CBs through cyclization of the 3′ and 5′ terminals of lASOs with a CB-sensitive peptide substrate (GFLG). The cyclization of lASOs could be greatly optimized on a large synthetic scale by designing a hairpin structure with additional 5- to 7-mer stem sequences, which could bring two terminals of ASOs close to each other. The cyclic topology of caged cASOs inhibited their binding to target mRNA and further mRNA degradation by RNase H1. The presence of CB activated the inert cASOs and induced target RNA digestion by RNase H1, and a significant activation effect of RNA cleavage (22.5-fold) using cASO$_{TCTP}$-CB was observed. This process could be blocked by addition of leupeptin because of its efficient inhibition of CB. The cASO-CBs were also expected to reduce their binding to off-target transcripts with significantly different K_d values compared with lASO, which could reduce the off-target effect of antisense therapy. Further cellular studies showed that cASO-CBs successfully achieved cell-specific downregulation of target genes (TCTP and LTBR) at the mRNA and protein levels in CB-rich PC-3 cancer cells. However, this did not happen in CB-deficient HUVECs and CB-suppressed PC-3 cells because of low levels of CB and weaker activation of cASO$_{TCTP}$-CB. Further xenograft nude mouse tumor model study indicated that cASO$_{TCTP}$-CB induced effective gene knockdown at the TCTP protein level in CB -rich PC-3 tumors and successfully achieved efficient suppression of tumor growth in comparison with non-CB-sensitive cASO$_{TCTP}$-GGGG and the NC. This study is the first attempt to apply enzyme-activatable cASOs in a nude mouse model for antitumor therapy with the assistance of an endogenous trigger.

Nonspecific immunostimulation of ASO drugs was one of the key side effects of antisense therapy. In this study, cASO-CB showed much weaker nonspecific immunostimulation, with up to 2-fold and 4-fold decreases in IL-6 and IFN-β levels, respectively, in comparison with the corresponding lASOs. Although a more detailed mechanism needs to be determined, the circulation strategy of ASOs might be a potential method for overcoming this inherent shortcoming of antisense therapy and greatly decreases the off-target effect in systemic administration of ASOs in the future. These results indicated that enzyme activation of cASOs would be a promising strategy for developing cell-specific ASO prodrugs for disease-related gene knockdown and cancer therapy.

The cyclization strategy of functional oligonucleotides is not limited to RNase H1-induced antisense effects, and cyclic oligonucleotides for gene knockdown or gene editing should also work in the presence of different specific triggers. Because cyclic oligonucleotides with the current circulation strategy will still have a tag at oligonucleotide terminals after enzymatic cleavage, any functional oligonucleotides should not be cyclized using this strategy when free terminals of oligonucleotides are required. In order to achieve scale synthesis of cyclic ASOs, our current strategy needs around 5 base-paired to hairpin stem to bring two ASO terminals close to each other and avoid oligomer formation. A new cyclization strategy needs to be developed for ASO cyclization if we do not want to introduce a terminal hairpin structure. In addition, current delivery of nucleic acid drugs is still very challenging. Even though cyclic phosphorothioated ASOs could be taken up by cells, a much high concentration (up to several micromolar) of naked ASOs was required. Here, oligonucleotide delivery agents were still used for cellular and animal experiments. Intratumoral administration of ASOs with the Entranster-*in vivo* agent was applied for evaluation of possible activation of cASOs with endogenous triggers. Currently, lipid nanoparticle (LNP) or bioconjugation (such as N-acetylgalactosamine conjugation) of oligonucleotide drugs are two main strategies for efficient oligonucleotide delivery, but most oligonucleotide drugs were enriched in the liver. In the future, development of new nucleic acid delivery technologies containing new organ-specific targeting motifs is expected to make systemic application of these enzyme-activatable cyclic oligonucleotides possible.

MATERIALS AND METHODS

Reagents and cell lines

All reagents and solvents were purchased from commercial suppliers without further purification. CB was purchased from Sino Biological

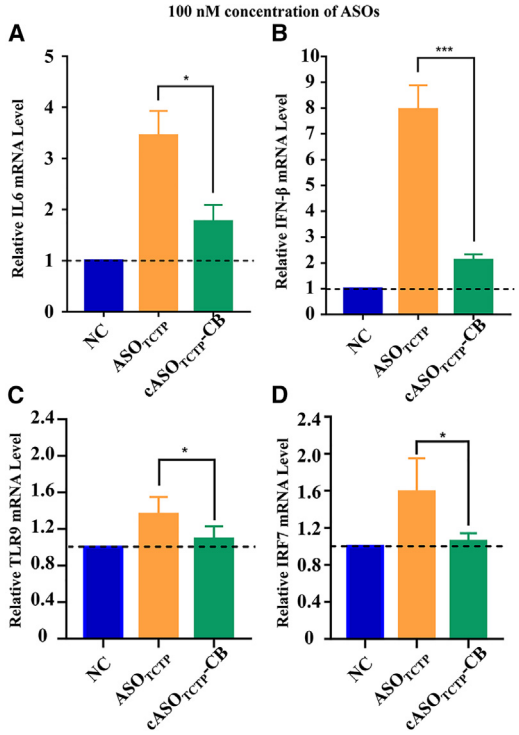

Figure 6. Evaluation of four immune indicators with lASO$_{TCTP}$ and cASO$_{TCTP}$-CB in PC-3 cells

(A–D) The relative IL-6 (A), IFN-β (B), TLR9 (C), and IRF7 (D) mRNA levels in PC-3 cells with transfection of ASO$_{TCTP}$ and cASO$_{TCTP}$-CB at 100 nM for 24 h. The IL-6, IFN-β, TLR9, and IRF7 mRNA levels were normalized to GAPDH RNA as the internal control using qRT-PCR. All data are presented as mean ± SEM (n ≥ 3). *p < 0.05, ***p < 0.001.

(10483-H08H). Caspase-3 was purchased from Abcam (ab52101). Peptidase was purchased from Shanghai Yuanye Bio-Technology (S10150). PC-3 cells and HUVECs were provided by the Xing Yang Lab, Peking University First Hospital.

Synthesis and purification of cyclic ASOs

The C6-NHS phosphoramidite linker (linker 1) was synthesized according to our previous report[44] (Figure S1). Phosphorothioate DNA oligonucleotides were synthesized using an ABI394 DNA/RNA synthesizer with the 3′-amino-modifier C7 CPG (TCTP sequence, 5′-AACTTGTTTCCTGCAGGTGA-3′; LTBR sequence, 5′-GTCACAGGGGCGGCACAGCT-3′; Table S1). Then linker 1 was coupled to the oligonucleotide sequence on the solid phase under the standard step of phosphoramidite chemistry. Then, 1 μmol of the above synthesized oligonucleotides on CPG (**1**) and 1.2 mg (∼2 equiv) synthesized peptides (6′-heptynoic acid-GFLGK/6′-heptynoic acid-GGGGK, **2a/2b**) were mixed in 40 μL dry N,N-dimethylformamide (DMF) with 2% (v/v) N,N-diisopropylethylamine (DIPEA), and the mixtures were shaken at 25°C for 24 h. The oligonucleotide CPGs were washed sequentially with DMF (3 × 1 mL) and CH_3CN (3 × 1 mL) and dried by rotary evaporation. After removing the Fmoc protection group of the 3′ terminal amino with piperidine, the peptide-oligonucleotide conjugates (ASO-CB/ASO-GGGG, **3a/3b**) were cleaved from oligonucleotide CPGs and further deprotected using 0.2 mL concentrated aqueous ammonium at 65°C for 2 h. These conjugates (**3a/3b**) were then purified by HPLC (Waters, Alliance e2695) using an XBridge BEH300 C18 column (Waters, 186003614) on a gradient of acetonitrile/0.05 M triethylamine acetate (TEAA) buffer (pH 7.0, A = TEAA buffer, B = acetonitrile; B: 10%–50% in 30 min; flow rate, 0.6 mL/min), and characterized by Electrospray Ionisation Mass Spectrometry (ESI-MS). The 3′-azidopropanoic acid NHS ester (linker 2) was synthesized as in previously reported methods[45] (Figure S1). The linker 2 (3 μmol) reacted with the purified peptide-oligonucleotide conjugates (ASO-CB/ASO-GGGG, **3a/3b**, 10 nmol) in a mixture solvent (50 μL 1× PBS and 50 μL DMSO) at 25°C for 24 h. The 3′-N_3-functionalized conjugates (lASO-CB/lASO-GGGG, **4a/4b**) were then purified by HPLC and characterized by ESI-MS. Finally, cASO-CB/cASO-GGGG (**5a/5b**) was constructed from the corresponding lASO-CB/lASO-GGGG via a CuAAC click reaction at 25°C for 4 h (in 200 μL mixed reaction solution of 6% CH_3CN/H_2O [v/v] supplemented with 5 μL $CuSO_4$ [20 mM], 6 μL tris(2-carboxyethyl)phosphine (TCEP) [20 mM], and 10 μL $NaHCO_3$ [200 mM]) (Figure S1). The cyclization products were purified by HPLC or gel recycling methods and further characterized by ESI-MS and PAGE gels.

Ring opening of cASO$_{TCTP}$-CB with CB

CB (10 μg/mL) was preactivated under 5 mM DTT at 37°C for 15 min. Then, 1 μM cASO$_{TCTP}$-CB was incubated under 1 μg/mL CB in enzyme assay buffer (25 mM MES [pH 5.0]) at 37°C for 1 h. Samples were allocated from the enzyme assay solution every 10 min. All allocated samples were mixed with gel loading buffer and then incubated at 95°C for 2 min to denature CB for the gel shift assay. A 20% native gel was prepared to represent enzyme cleavage for cASO$_{TCTP}$-CBs (Figure 3A). The gels were run in 1× tris-borate-EDTA (TBE) buffer at 200 V for 1 h and then stained with SYBR Gold nucleic acid dye (Invitrogen) for 5 min. The stained gels were imaged by a chemiluminescence gel imaging system (ChemiDoc XRS). The percentage of cleaved cASO$_{TCTP}$-CB was analyzed and quantitated by Image Lab software.

Interaction of lASO$_{TCTP}$-CB or cASO$_{TCTP}$-CB with CB

The affinity of the GFLG tetrapeptide to Cathepsin B was examined in the linear ASO or cyclic ASO, respectively. lASO$_{TCTP}$-CB or cASO$_{TCTP}$-CB at 0.5, 1, 2, and 4 μM was incubated with CB (1 μg/mL) in MES buffer (pH = 5.0) at 37°C for 1 h. Then, the cleavage results were analyzed by 12% denaturing PAGE, and the grayscale quantitative analysis of the cleaved bands was recorded. Finally, the Km values of substrates (lASO$_{TCTP}$-CB or cASO$_{TCTP}$-CB) to Cathepsin B cleavage reaction were fitted according to the Lineweaver-Burk plot:

$$1/V = Km/Vmax[S] + 1/Vmax \quad \text{(Equation 1)}$$

Here, the grayscale values of product bands were used in a 1-h cleavage process to replace the V value in the equation (Figure S2).

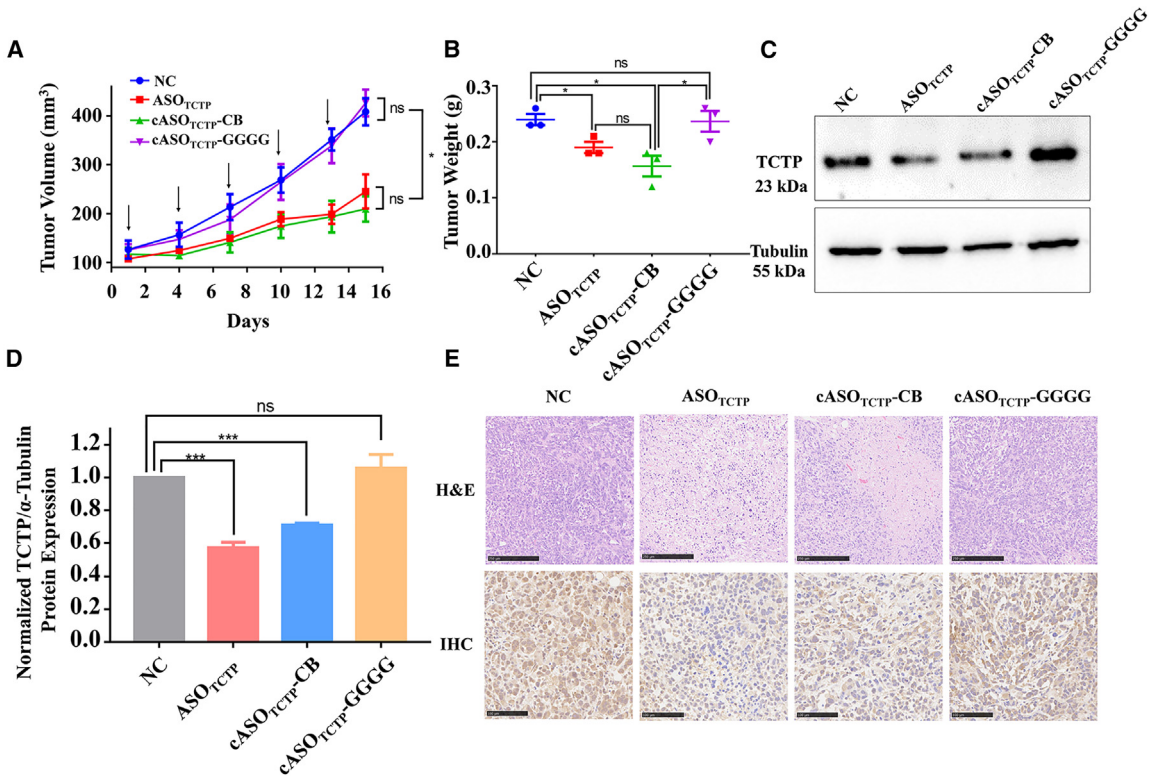

Figure 7. *In vivo* TCTP gene silencing and anti-tumor effects with $cASO_{TCTP}$-CB

(A) Relative tumor volume curves of each group after intratumoral injection of saline (0.9%), ASO_{TCTP}, $cASO_{TCTP}$-CB, and $cASO_{TCTP}$-GGGG (3 nmol ASOs per dose), respectively. Each injection is indicated by a black arrow. (B) The corresponding tumor weight after mice were sacrificed. Western blot analysis (C) and gray quantitative (D) of TCTP protein expression in tumor tissues. (E) H&E histological image (scale bar = 250 μm) and IHC of TCTP protein expression in the tumor tissues (scale bar =100 μm). The ASOs used in the nude mouse model were transfected by Entranster-*in vivo*. All data are presented as mean ± SEM (n = 3). *p < 0.05 ***p < 0.001.

MST analysis

A 46-mer Cy5-labeled target RNA (Cy5-RNA) truncated from TCTP mRNA was designed and synthesized. The binding affinity of lASO or cyclic ASO to the truncated Cy5-RNA was measured using MST by Monolith NT.115 (NanoTemper). Cy5-RNA (100 nM) was incubated with lASO (0.3 nM–10 μM) or cyclic ASO (2.4 nM–80 μM) at 37°C for 15 min. The mixture systems were analyzed using MST, and the data were fitted with the K_d model (Figure S6).

Inhibition assay for CB cleavage

CB was pre-activated as described previously. Activated CB was pre-mixed with different concentrations of leupeptin (0.25, 2, 4, and 10 μM) at 37°C for 5 min. Then, 1 μM $cASO_{TCTP}$-CB and 1 μg/mL CB were incubated with leupeptin at different concentrations in 25 mM MES buffer (pH 5.0) at 37°C for 1 h. Native gels were used to analyze and quantify leupeptin cleavage inhibition according to the abovementioned method (Figure 3B).

RNase H1-mediated RNA cleavage assay

Before the RNA cleavage assay, $cASO_{TCTP}$-CB was mixed with 1 μg/mL CB at 37°C for 1 h. Then, the 46-mer Cy3-labeled target RNA (Cy3-RNA) truncated from TCTP mRNA was incubated with CB -cleaved $cASO_{TCTP}$-CB and $cASO_{TCTP}$-CB as well as positive control $lASO_{TCTP}$ in 1× RNase H1 buffer (20 mM Tris-HCl, 20 mM KCl, 10 mM $MgCl_2$, 0.1 mM EDTA, and 0.1 mM dithiothreitol [pH 8.0]) at a concentration of 4 μM RNA and 0.1 μM ASO at 37°C for 20 min. Then, RNase H1 was added to the above mixture solution at a final concentration of 0.5 U/μL. 2 μL reaction solution was allocated each time at four time points (10, 25, 40, and 60 min) and quenched and analyzed in 20% denaturing PAGE gels (Figure S6). The signal of Cy3-RNA and its cleaved bands was detected upon excitation at 488 nm using Amersham Typhoon RGB. The gray quantitative of the Cy3 signal was analyzed using ImageJ software.

Transfection with cASO-CB and qRT-PCR

PC-3 cells were cultured in RPMI 1640 medium (M&C) supplemented with 10% fetalbovine serum (FBS; Pan), penicillin, and streptomycin at 37°C and 5% CO_2. HUVECs were cultured in DMEM (M&C) supplemented with 10% FBS, penicillin, and streptomycin at 37°C and 5% CO_2. PC-3 cells were plated in 24-well plates at a density of 2×10^5 cells per well. For dose-dependent gene regulation (including TCTP and LTBR), PC-3 cells were transfected with ASO or cASO-CB using Lipofectamine 2000 at 30, 60 and 100 nM ASOs, respectively, and the cells were cultured for

48 h before RT-PCR analysis. For time-dependent TCTP gene regulation, PC-3 cells were transfected with ASO_{TCTP} and $cASO_{TCTP}$-CB at 100 nM using Lipofectamine 2000 and cultured for 24, 36, 48, and 60 h before cell lysis for RT-PCR analysis. For ASO_{LTBR} and $cASO_{LTBR}$-CB, PC-3 cells were transfected using Lipofectamine 2000 with 30 nM of ASOs and cultured for 12, 24, 36, 48, and 60 h before cell lysis for RT-PCR analysis. Total RNA was extracted from PC-3 cells using Biozol reagent (Biomiga). Respective cDNAs were obtained from 300 ng of RNA using HiScript III Q RT SuperMix for PCR (Vazyme) and real-time PCR was carried out using GoTaq qPCR Master Mix (Promega) according to the standard manufacturer's protocol.

CB-abundant PC-3 cells and CB-deficient HUVECs were plated in 6-well plates at a density of 5×10^5 cells per well and incubated for 24 h. ASO_{TCTP} or $cASO_{TCTP}$-CB was then transfected into these two different cell lines at a final concentration of 100 nM using Lipofectamine 2000. After 48 h of incubation, total RNA was extracted from PC-3 cells and HUVECs by Biozol reagent (Biomiga). The RT-PCR procedure was the same as the abovementioned protocol. Then, TCTP gene expression was normalized to 18S rRNA, and LTBR gene expression was normalized to the HPRT gene. In addition, the four indicator genes (IL-6, IFN-β, TLR9 and IRF7) of nonspecific immunostimulation were also analyzed according to the above procedures. All primers used in these studies are listed in Table S2.

Western blot assay

PC-3 cells and HUVECs, transfected with ASO_{TCTP} and $cASO_{TCTP}$-CB as described, were washed with 1× PBS and then lysed in RIPA lysis buffer supplemented with 1% proteinase inhibitor. The lysates were centrifuged at 12,000 × *g* for 20 min. Total proteins were quantified by BCA Protein Assay Kit. 80 μg total protein was loaded on an SDS-PAGE gel for electrophoresis, and the proteins on the gel were then transferred to polyvinylidene difluoride membranes. These membranes were incubated with 1:1,000 anti-TCTP polyclonal antibody (Abcam) for 24 h at 4°C after being blocked with 5% skimmed milk for 1 h. A peroxidase-conjugated secondary antibody (Sangon Biotech, Shanghai, China) was subsequently used on these membranes for 1 h at room temperature. Then, specific protein bands were detected on the ChemiDoc XRS System (Bio-Rad) using the enhanced chemiluminescent detection reagent kit (Thermo Scientific). The relative protein levels of TCTP and LTBR were normalized to β-actin and GAPDH, respectively, using ImageJ analysis software. The final western blot quantitative results were analyzed for at least three independent experiments.

ELISA

PC-3 cells were transfected with siRNA-targeted CB for 48h and then lysed in RIPA lysis buffer. The lysates were centrifuged at 12,000 × *g* for 20 min to collect the total proteins. Expression of CB was subsequently determined using the Human-CTSB (CB) ELISA Kit (Solarbio) according to the standard manufacturer's protocol. The final quantitative results were analyzed for at least three independent experiments.

In vivo TCTP gene knockdown and tumor growth inhibition

Six-week-old BALB/c male nude mice (Department of Laboratory Animal Science of the Peking University Health Science, Beijing, China) were used to construct the PC-3 xenografted models by subcutaneous injection of 5×10^6 PC-3 cells under the right pads. All nude mice were randomly divided into four groups (n = 3) when the tumor volume grew to approximately 100 mm^3. Saline (0.9%), ASO_{TCTP}, $cASO_{TCTP}$-CB, or $cASO_{TCTP}$-GGGG was injected intratumorally with a 1:2 ratio of ASOs and commercial transfection reagent (Entranster-*in vivo*) every 3 days. All mice were administered 3 nmol ASOs per injection for five consecutive injections. The tumor size was measured using a caliper, and the tumor volume was calculated as follows:

$$V = L \times W^2/2, \quad \text{(Equation 2)}$$

where L is the longest diameter and W the shortest diameter.

Tumor size and mouse body weight were measured every 3 days. Two days after the last injection, the animals were sacrificed to harvest tumors for imaging, and the tumor weight was measured and analyzed. The expression level of TCTP protein in tumor tissues was analyzed using western blotting and IHC. In addition, the pathological changes in tumors were analyzed through H&E staining.

DATA AND CODE AVAILABILITY

All supplemental figures, tables, and characterization are included in the supplemental information. All animal experiments were approved by the Committee for Animal Research of Peking University (permission certificate LA2021302). The specific pathogen-free (SPF)-grade male nude mice (6–8 weeks old) were obtained from Wantonglihua (China) and maintained at the Department of Laboratory Animal Science, Peking University Health Science Center.

SUPPLEMENTAL INFORMATION

Supplemental information can be found online at https://doi.org/10.1016/j.omtn.2023.07.022.

ACKNOWLEDGMENTS

This work was supported by the National Natural Science Foundation of China (grants 22277003, 81821004, 22077005, 22107004, and 22077008), the National Key R&D Program of China (2022YFC2303700), and the Open Fund of the State Key Laboratory of Pharmaceutical Biotechnology, Nanjing University, China (grant KF-202205).

AUTHOR CONTRIBUTIONS

Z.W. contributed to synthesis of cyclic oligonucleotides and solution and cellular studies and participated in animal experiments. X.F. contributed to animal experiments. G.M. participated in western blot experiments. X.Z. participated in the LTBR experiment. Q.W. and J.W. were involved in the assay study. X.T. designed and directed the whole study. All authors contributed to manuscript writing.

DECLARATION OF INTERESTS

The authors declare no competing interests.

REFERENCES

1. Meng, S., Zhou, H., Feng, Z., Xu, Z., Tang, Y., Li, P., and Wu, M. (2017). CircRNA: functions and properties of a novel potential biomarker for cancer. Mol. Cancer *16*, 94–102.
2. Ebbesen, K.K., Kjems, J., and Hansen, T.B. (2016). Circular RNAs: Identification, biogenesis and function. Biochim. Biophys. Acta *1859*, 163–168.
3. Darrah, K., Wesalo, J., Lukasak, B., Tsang, M., Chen, J.K., and Deiters, A. (2021). Small Molecule Control of Morpholino Antisense Oligonucleotide Function through Staudinger Reduction. J. Am. Chem. Soc. *143*, 18665–18671.
4. Griepenburg, J.C., Rapp, T.L., Carroll, P.J., Eberwine, J., and Dmochowski, I.J. (2015). Ruthenium-Caged Antisense Morpholinos for Regulating Gene Expression in Zebrafish Embryos. Chem. Sci. *6*, 2342–2346.
5. Yang, L., von Trentini, D., Kim, H., Sul, J.Y., Eberwine, J.H., and Dmochowski, I.J. (2021). Photoactivatable Circular Caged Oligonucleotides for Transcriptome In Vivo Analysis (TIVA). ChemPhotoChem *5*, 940–946.
6. Debart, F., Dupouy, C., and Vasseur, J.J. (2018). Stimuli-responsive oligonucleotides in prodrug-based approaches for gene silencing. Beilstein J. Org. Chem. *14*, 436–469.
7. Jahns, H., Degaonkar, R., Podbevsek, P., Gupta, S., Bisbe, A., Aluri, K., Szeto, J., Kumar, P., LeBlanc, S., Racie, T., et al. (2021). Small circular interfering RNAs (sciRNAs) as a potent therapeutic platform for gene-silencing. Nucleic Acids Res. *49*, 10250–10264.
8. Hagiwara, K., Honma, M., Harumoto, T., Harada, K., Sawada, T., Yamamoto, J., and Shinohara, F. (2020). Development of Prodrug Type Circular siRNA for In Vivo Knockdown by Systemic Administration. Nucleic Acid Therapeut. *30*, 346–364.
9. Kimura, Y., Shu, Z., Ito, M., Abe, N., Nakamoto, K., Tomoike, F., Shuto, S., Ito, Y., and Abe, H. (2020). Intracellular build-up RNAi with single-strand circular RNAs as siRNA precursors. Chem. Commun. *56*, 466–469.
10. Yamazoe, S., Liu, Q., McQuade, L.E., Deiters, A., and Chen, J.K. (2014). Sequential gene silencing using wavelength-selective caged morpholino oligonucleotides. Angew Chem. Int. Ed. Engl. *53*, 10114–10118.
11. Yamazoe, S., Shestopalov, I.A., Provost, E., Leach, S.D., and Chen, J.K. (2012). Cyclic Caged Morpholinos: Conformationally Gated Probes of Embryonic Gene Function. Angew Chem. Int. Ed. Engl. *51*, 6908–6911.
12. Wu, L., Wang, Y., Wu, J., Lv, C., Wang, J., and Tang, X. (2013). Caged circular antisense oligonucleotides for photomodulation of RNA digestion and gene expression in cells. Nucleic Acids Res. *41*, 677–686.
13. Wang, Y., Wu, L., Wang, P., Lv, C., Yang, Z., and Tang, X. (2012). Manipulation of gene expression in zebrafish using caged circular morpholino oligomers. Nucleic Acids Res. *40*, 11155–11162.
14. Griepenburg, J.C., Ruble, B.K., and Dmochowski, I.J. (2013). Caged oligonucleotides for bidirectional photomodulation of let-7 miRNA in zebrafish embryos. Bioorg. Med. Chem. *21*, 6198–6204.
15. Yang, L., Kim, H.B., Sul, J.Y., Yeldell, S.B., Eberwine, J.H., and Dmochowski, I.J. (2018). Efficient Synthesis of Light-Triggered Circular Antisense Oligonucleotides Targeting Cellular Protein Expression. Chembiochem *19*, 1250–1254.
16. Deodato, D., and Dore, T.M. (2020). Practical Synthesis of Quinoline-Protected Morpholino Oligomers for Light-Triggered Regulation of Gene Function. Molecules *25*, 2078–2089.
17. Jin, C., Ei-Sagheer, A.H., Li, S., Vallis, K.A., Tan, W., and Brown, T. (2022). Engineering Enzyme-Cleavable Oligonucleotides by Automated Solid-Phase Incorporation of Cathepsin B Sensitive Dipeptide Linkers. Angew Chem. Int. Ed. Engl. *61*, e202114016. https://doi.org/10.1002/anie.202114016.
18. Yamazoe, S., McQuade, L.E., and Chen, J.K. (2014). Nitroreductase-activatable morpholino oligonucleotides for *in vivo* gene silencing. ACS Chem. Biol. *9*, 1985–1990.
19. Yang, L., Eberwine, J.H., and Dmochowski, I.J. (2020). Caspase-Activated Oligonucleotide Probe. Bioconjugate Chem. *31*, 2172–2178.
20. Yang, L., and Dmochowski, I.J. (2021). Conditionally Activated ("Caged") Oligonucleotides. Molecules *26*, 1481–1495.
21. Zhang, H.H., Zhao, L.D., Zuo, P., Yin, B.C., and Ye, B.C. (2020). A telomerase-responsive nanoprobe with theranostic properties in tumor cells. Talanta *215*, 120898.
22. Shim, M.K., Yoon, H.Y., Ryu, J.H., Koo, H., Lee, S., Park, J.H., Kim, J.H., Lee, S., Pomper, M.G., Kwon, I.C., and Kim, K. (2016). Cathepsin B-Specific Metabolic Precursor for In Vivo Tumor-Specific Fluorescence Imaging. Angew Chem. Int. Ed. Engl. *55*, 14698–14703.
23. Zhong, Y.J., Shao, L.H., and Li, Y. (2013). Cathepsin B-cleavable doxorubicin prodrugs for targeted cancer therapy (Review). Int. J. Oncol. *42*, 373–383.
24. Shim, M.K., Park, J., Yoon, H.Y., Lee, S., Um, W., Kim, J.H., Kang, S.W., Seo, J.W., Hyun, S.W., Park, J.H., et al. (2019). Carrier-free nanoparticles of cathepsin B-cleavable peptide-conjugated doxorubicin prodrug for cancer targeting therapy. J. Contr. Release *294*, 376–389.
25. Shim, M.K., Moon, Y., Yang, S., Kim, J., Cho, H., Lim, S., Yoon, H.Y., Seong, J.K., and Kim, K. (2020). Cancer-specific drug-drug nanoparticles of pro-apoptotic and cathepsin B-cleavable peptide-conjugated doxorubicin for drug-resistant cancer therapy. Biomaterials *261*, 120347.
26. Song, S.J., Lee, S., Lee, Y., and Choi, J.S. (2016). Enzyme-responsive destabilization of stabilized plasmid-lipid nanoparticles as an efficient gene delivery. Eur. J. Pharmaceut. Sci. *91*, 20–30.
27. Lee, J.S., Groothuis, T., Cusan, C., Mink, D., and Feijen, J. (2011). Lysosomally cleavable peptide-containing polymersomes modified with anti-EGFR antibody for systemic cancer chemotherapy. Biomaterials *32*, 9144–9153.
28. Aggarwal, N., and Sloane, B.F. (2014). Cathepsin B: multiple roles in cancer. Proteonomics Clin. Appl. *8*, 427–437.
29. Ni, Y., Hai, Z., Zhang, T., Wang, Y., Yang, Y., Zhang, S., and Liang, G. (2019). Cathepsin B Turning Bioluminescence "On" for Tumor Imaging. Anal. Chem. *91*, 14834–14837.
30. Dheer, D., Nicolas, J., and Shankar, R. (2019). Cathepsin-sensitive nanoscale drug delivery systems for cancer therapy and other diseases. Adv. Drug Deliv. Rev. *151–152*, 130–151.
31. Miller, K., Erez, R., Segal, E., Shabat, D., and Satchi-Fainaro, R. (2009). Targeting bone metastases with a bispecific anticancer and antiangiogenic polymer-alendronate-taxane conjugate. Angew Chem. Int. Ed. Engl. *48*, 2949–2954.
32. Wang, Q., Yu, L., Wong, R.C.H., and Lo, P.C. (2019). Construction of cathepsin B-responsive fluorescent probe and photosensitizer using a ferrocenyl boron dipyrromethene dark quencher. Eur. J. Med. Chem. *179*, 828–836.
33. Baici, A., Gyger-Marazzi, M., and MJEJoB. (1982). The slow, tight-binding inhibition of cathepsin B by leupeptin. A hysteretic effect. Eur. J. Biochem. *129*, 33–41.
34. Tang, X., Su, M., Yu, L., Lv, C., Wang, J., and Li, Z. (2010). Photomodulating RNA cleavage using photolabile circular antisense oligodeoxynucleotides. Nucleic Acids Res. *38*, 3848–3855.
35. Karaki, S., Benizri, S., Mejías, R., Baylot, V., Branger, N., Nguyen, T., Vialet, B., Oumzil, K., Barthélémy, P., and Rocchi, P. (2017). Lipid-oligonucleotide conjugates improve cellular uptake and efficiency of TCTP-antisense in castration-resistant prostate cancer. J. Contr. Release *258*, 1–9.
36. Or, Y.Y.Y., Chung, G.T.Y., To, K.F., Chow, C., Choy, K.W., Tong, C.Y.K., Leung, A.W.C., Hui, A.B.Y., Tsao, S.W., Ng, H.K., et al. (2010). Identification of a novel 12p13.3 amplicon in nasopharyngeal carcinoma. J. Pathol. *220*, 97–107.
37. Zhou, P., Fang, X., McNally, B.A., Yu, P., Zhu, M., Fu, Y.-X., Wang, L., Liu, Y., and Zheng, P. (2009). Targeting Lymphotoxin-Mediated Negative Selection to Prevent Prostate Cancer in Mice with Genetic Predisposition, *106*, pp. 17134–17139.
38. Wolf, M.J., Seleznik, G.M., Zeller, N., and Heikenwalder, M. (2010). The unexpected role of lymphotoxin beta receptor signaling in carcinogenesis: from lymphoid tissue formation to liver and prostate cancer development. Oncogene *29*, 5006–5018.
39. Lenert, P.S. (2010). Classification, mechanisms of action, and therapeutic applications of inhibitory oligonucleotides for Toll-like receptors (TLR) 7 and 9. Mediat. Inflamm. *2010*, 986596.
40. Gubu, A., Su, W., Zhao, X., Zhang, X., Fan, X., Wang, J., Wang, Q., and Tang, X. (2021). Circular Antisense Oligonucleotides for Specific RNase-H-Mediated

microRNA Inhibition with Reduced Off-Target Effects and Nonspecific Immunostimulation. J. Med. Chem. *64*, 16046–16055.

41. Agrawal, S., and Kandimalla, E.R. (2004). Role of Toll-like receptors in antisense and siRNA [corrected]. Nat. Biotechnol. *22*, 1533–1537.

42. Sarvestani, S.T., Stunden, H.J., Behlke, M.A., Forster, S.C., McCoy, C.E., Tate, M.D., Ferrand, J., Lennox, K.A., Latz, E., Williams, B.R.G., and Gantier, M.P. (2015). Sequence-dependent off-target inhibition of TLR7/8 sensing by synthetic microRNA inhibitors. Nucleic Acids Res. *43*, 1177–1188.

43. Pépin, G., Ferrand, J., and Gantier, M.P. (2017). Assessing the Off-Target Effects of miRNA Inhibitors on Innate Immune Toll-Like Receptors. In Drug Target miRNA: Methods and Protocols, M.F. Schmidt, ed. (Springer New York), pp. 127–135.

44. Zhang, J., Jing, N., Fan, X., and Tang, X. (2020). Photoregulation of Gene Expression with Amantadine-Modified Caged siRNAs through Host-Guest Interactions. Chem. Eur J. *26*, 14002–14010.

45. Bhadra, J., Pattanayak, S., Khan, P.P., Kundu, J., and Sinha, S. (2016). Internal Oligoguanidinium-Based Cellular Transporter Enhances Antisense Efficacy of Morpholinos in In Vitro and Zebrafish Model. Bioconjugate Chem. *27*, 2254–2259.